Mixed-mode fatigue crack propagation simulation by means of G_{eq} and walker models of the structural steel S355

Xin, Haohui; Liu, Jielin; Correia, José A.F.O.; Berto, Filippo; Veljkovic, Milan; Qian, Guian

DOI
10.1016/j.tafmec.2022.103717

Publication date
2023

Document Version
Final published version

Published in
Theoretical and Applied Fracture Mechanics

Theoretical and Applied Fracture Mechanics 123 (2023) 103717

Contents lists available at ScienceDirect

Theoretical and Applied Fracture Mechanics

journal homepage: www.elsevier.com/locate/tafmec

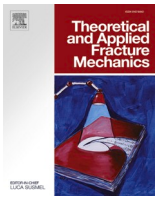

Mixed-mode fatigue crack propagation simulation by means of G_{eq} and walker models of the structural steel S355

Haohui Xin [a], Jielin Liu [a], José A.F.O. Correia [a,b,d,*], Filippo Berto [a,c], Milan Veljkovic [d], Guian Qian [e]

[a] Department of Civil Engineering, Xi'an Jiaotong University, Xi'an 710116, China
[b] CONSTRUCT & LAETA/INEGI, Faculty of Engineering, University of Porto, 4200-465 Porto, Portugal
[c] Department of Mechanical and Industrial Engineering, Norwegian University of Science and Technology (NTNU), Norway
[d] Department of Engineering Structures, Delft University of Technology, Delft, the Netherlands
[e] State Key Lab. of Nonlinear Mechanics, Institute of Mechanics, Chinese Academy of Sciences, Beijing 100190, China

ARTICLE INFO

Keywords:
Mixed mode fatigue crack propagation
Equivalent energy release rate ()
Extended finite element method (XFEM)
Virtual Crack Closure Technology (VCCT)
Walker equation

ABSTRACT

In this paper, a numerical simulation method of mixed-mode fatigue crack propagation was explored using the extended finite element method (XFEM) and the Virtual Crack Closure Technique (VCCT). Both 2D and 3D numerical models were selected to simulate the fatigue crack propagation of steel specimens. Two coefficients were proposed to calculate the equivalent energy release rate (G_{eq}) for a better simulation of the mixed-mode fatigue crack propagation of S355 steel. The Walker equation and the calculation formula of G_{eq} were realized by a user-defined subroutine. A set of optimal correction coefficients of mode II energy release rate (G_{II}) and mode III energy release rate (G_{III}) were quantitatively comparing the simulation results and test data. The results will contribute to fatigue crack propagation prediction of steel structures in the civil engineering field.

1. Introduction

Fatigue damage is a common failure phenomenon in engineering structures, and it is one of the most important factors restricting the normal service of structures. To accurately evaluate the residual service life of steel structures, it is very important to accurately evaluate the fatigue life of the fatigue crack propagation period. Steel grade S355 is widely used in steel structures around the world, thus the investigation of its fatigue crack propagation behavior is very important.

In recent years, the fatigue crack propagation of steel structures was investigated experimentally and numerically. Mohabeddine et al. [1] proposed a model to predict the fatigue crack growth of carbon fiber reinforced polymer (CFRP) repaired Center-Cracked Tension (CCT) steel specimens. A coefficient β before the stress intensity factor (SIF) is proposed to better predict the mode I fatigue crack propagation of the CFRP repaired steel plate specimens. The asymmetric method and simplified symmetric method are proposed by Wang et al. [2] to predict the crack propagation behavior of un-strengthened and FRP strengthened steel beams with double-edged cracks. Yu et al. [3] investigated the effect of bond length, bond width, CFRP laminate modulus, and adhesive shear modulus on the SIF value at the crack tip of strengthened steel plates using the boundary element method (BEM).

However, the steel structures often suffer complicated external load, then mixed-mode fatigue crack propagation often appeared. The stress field at the tip of the mixed-mode fatigue crack is quite complex, it is necessary to simulate the fatigue crack propagation exposed to mixed-mode loading using numerical methods. Several scholars have studied the mixed-mode fatigue crack propagation experimentally and numerically in recent years. Zhu et al. [4] provided a system-atic review and comparison of the evaluation method of notch fatigue. Dantas et al. [5] conducted fatigue crack propagation tests of S355 steel specimens exposed to mixed-mode I + II with different load ratios. The results showed that the crack propagation rate slows down with the increase of the loading angle. Rozumek et al. [6] experimentally investigated the fatigue crack propagation of S355J0 steel under mixed-mode I + III loading. The fatigue life of the mixed-mode I + III fatigue specimens decreased with the increase of the ratio of torsional torque to bending torque. Rege et al. [7] studied the phenomenon of fatigue crack

* Corresponding author at: Department of Civil Engineering, Xi'an Jiaotong University, Xi'an 710116, China. CONSTRUCT & LAETA/INEGI, Faculty of Engineering, University of Porto, 4200-465 Porto, Portugal.
E-mail addresses: xinhaohui@xjtu.edu.cn (H. Xin), xjtljl@stu.xjtu.edu.cn (J. Liu), jacorreia@inegi.up.pt (J.A.F.O. Correia), filippo.berto@ntnu.no (F. Berto), M.Veljkovic@tudelft.nl (M. Veljkovic), qianguian@imech.ac.cn (G. Qian).

https://doi.org/10.1016/j.tafmec.2022.103717
Received 4 August 2022; Received in revised form 29 October 2022; Accepted 2 December 2022
Available online 9 December 2022

Table 1
Material properties of S355 steel [26].

Young Modulus(E)	Yield Strength(f_y)	Tensile Strength (f_u)	Hardness
GPa	*MPa*	*MPa*	*HV10*
211.6	367	579	151.28

Table 2
The material composition of S355 steel [26].

C	Cu	Mn	N	P	S	Si
%	%	%	%	%	%	%
0.16	0.2	1.28	0.009	0.03	0.02	0.3

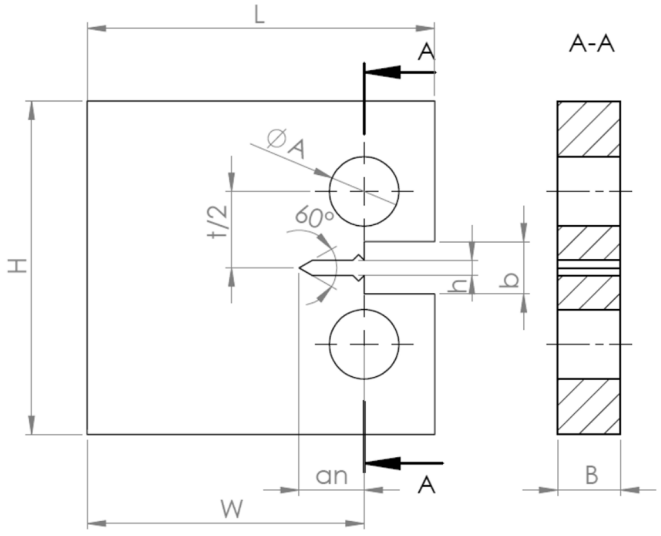

Fig. 1. Geometry of compact tensile specimens [5].

propagation retardation due to overload and concluded that overload will lead to the delay of fatigue crack propagation under mixed loading. Pedrosa et al. [8] proposed a unified two-stage fatigue methodology to assess the fatigue crack propagation of S355 steel considering the plasticity induced crack closure effect. Sajith et al. [9] studied the equivalent stress intensity factor ranges (ΔK_{eq}) of mixed-mode fatigue cracks in aluminum 6061-T6 and concluded that Irwin's equivalent stress intensity factor model is most consistent with the experimental data. Lesiuk et al. [10] proposed a numerical procedure to evaluate the I + II mixed mode fatigue propagation. Qi et al. [11–12] proposed two different prediction models based on low-cycle fatigue properties without completing the high-cycle fatigue crack growth test to predict the relationship between fatigue crack propagation rate and J-integral range of mixed-mode I + II cracks. Zhu et al. [13] proposed a probabilistic procedure for modeling multiple surface crack propagation and coalescence by incorporating Monte Carlo simulation with experimental evidence. Chen et al. [14] experimentally studied the mixed-mode fatigue crack growth life of CCT specimens with five inclined angles repaired with CFRP. Barsoum et al. [15] predicted the fracture initiation, crack propagation, and mode of crack extension accurately based on extended finite element method (XFEM). Pavlou et al. [16] proposed a methodology to predict the direction and the propagation rate of mixed-mode fatigue cracks based on the principle of the minimum potential energy. Yu et al. [17] proposed a time-based fatigue crack growth method for steel bridges under traffic loading that does not require cycle counting. Heng et al. [18] proposed a probabilistic fatigue crack growth (PFCG) model including toe-to-deck (TTD) cracking and root-to-deck (RTD) cracking under mixed failure modes. Li et al. [19] simulated the fatigue crack propagation of CFRP repaired steel plates with inclined cracks based on FEM. Huang et al. [20] studied fatigue crack growth in CFRP-repaired four-point bending specimens and concluded that the repair effect of CFRP strips becomes more significant with the decrease of the KII/KI ratio. Aljabar et al. [21] studied the fatigue crack propagation of steel plates with initially inclined cracks strengthened by different CFRP plates with different mechanical properties.

The most important factor to simulate the fatigue crack is to accurately define the equivalent crack driving force. In the engineering application, the commercial software is relatively convenient to model complex joints. The authors [22] evaluate the load ratio effects on the pure mode I fatigue crack propagation rate of structural steel grades S355 and S690 by using the extended finite element method (XFEM) [23] based on Virtual Crack Closure Technique (VCCT) [24] and fatigue crack propagation rate equation [25]. To consider the effect of the mean stress, the Walker equation [25] was used to calculate the fatigue crack propagation rate. The equivalent energy release rate is assumed as the linear sum of three components of the energy release rate in the author's previous publication. This assumption is proved to be not suitable for mixed-mode fatigue crack propagation. Two modification coefficients before mode II energy release rate (G_{II}) and mode III energy release rate

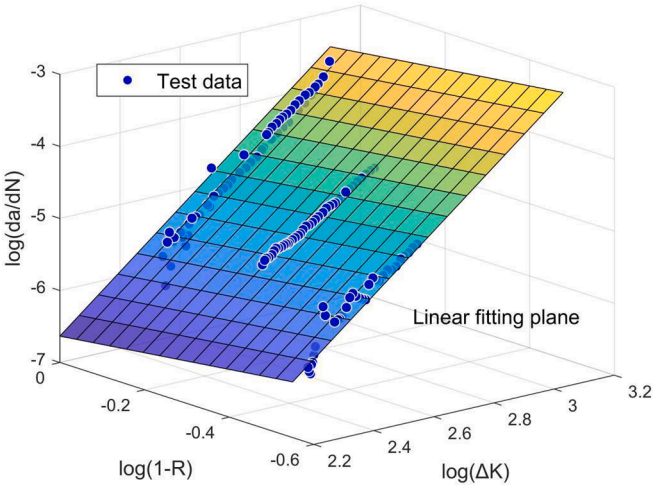

Fig. 2. Fitting of test data.

Table 4
Coefficients of Walker Equation.

Parameters	Statistical values	S355
$\log(C_0)$	Average	−14.34
γ	Average	0.789
m	Average	3.503
R^2		0.9515
RMSE		0.1269
SSE		6.118

Table 3
Dimension of compact tension specimens (mm) [5].

Specimen	R	W	L	H	A	B	b	an	h	t/2
1	0.5	50	62.5	60	12.5	11.3	9.4	11.7	2.75	13.75
2	0.7	49.84	62.3	59.8	12.5	10.27	9.4	11.8	2.94	13.71

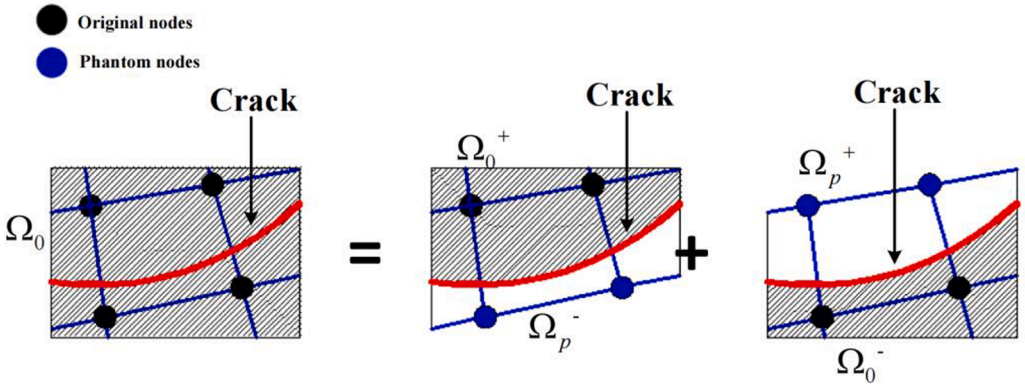

Fig. 3. The schematic of the phantom node method [28].

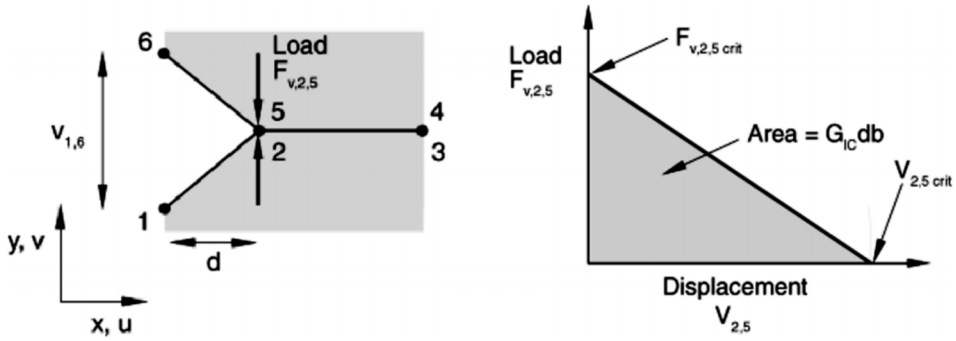

Fig. 4. Schematic finite element representation of the VCCT method [24].

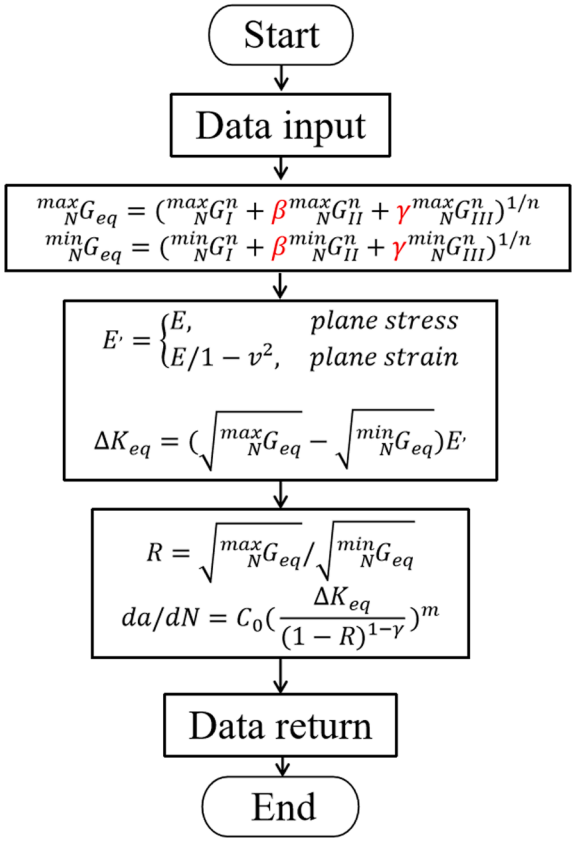

Fig. 5. Implementation flow chart of the user subroutine.

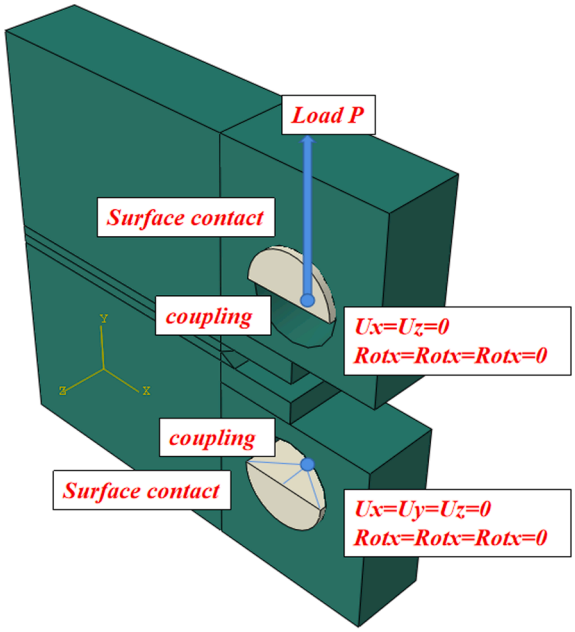

Fig. 6. Boundary conditions of compact tensile specimen.

(G_{III}) of the formula to calculate the equivalent energy release rate (G_{eq}) are introduced in this paper to better calculate the equivalent energy release rate exposed to mixed-mode loading.

In this paper, the median material coefficient of the Walker equation and the material coefficient with the 95 % guarantee rate were used to simulate mixed-mode fatigue crack propagation to consider the scatter

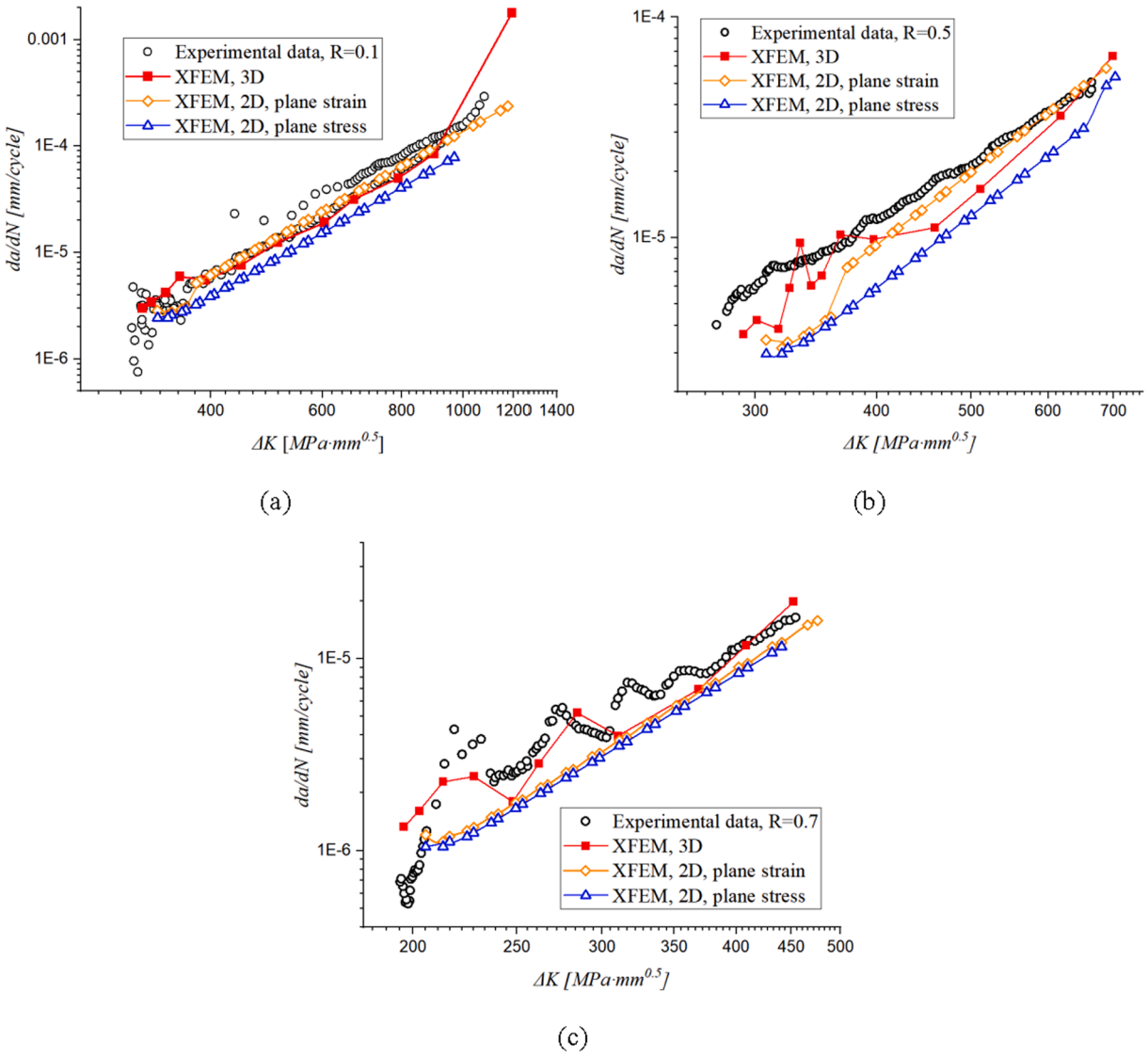

Fig. 7. Comparison between pure mode I fatigue crack propagation simulation results and test data.

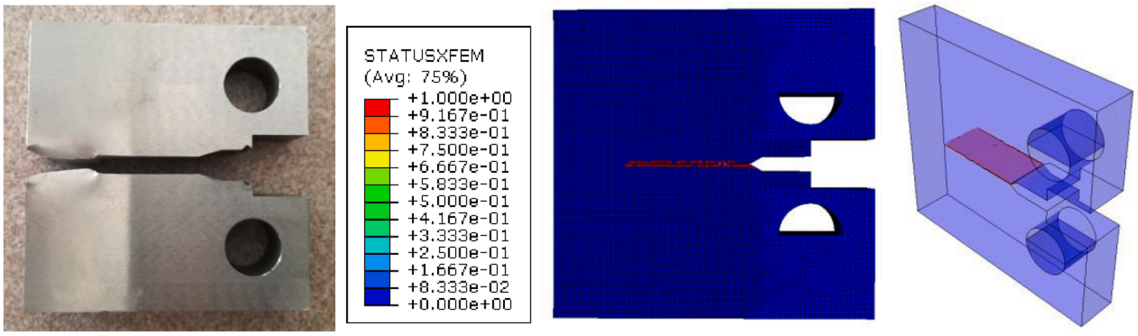

Fig. 8. Failure modes of numerical simulation and experimental observation (R = 0.5).

Table 5
Coefficient of Walker equation with 95% guarantee rate.

95 % guarantee rate	$\log(C_0)$	γ	m
Upper limit	−13.23	3.202	0.7852
Lower limit	−13.42	3.086	0.8398

of test results. During the simulation, the revised equivalent energy release rate G_{eq} were realized by a user-defined subroutine. The 2D and 3D finite element models were used to simulate the fatigue crack propagation, and numerical simulation results were compared with the test data to obtain the proposed coefficients. Finally, the effects of the revised coefficient on pure mode I fatigue crack growth were checked by comparing the test data with the simulation results again.

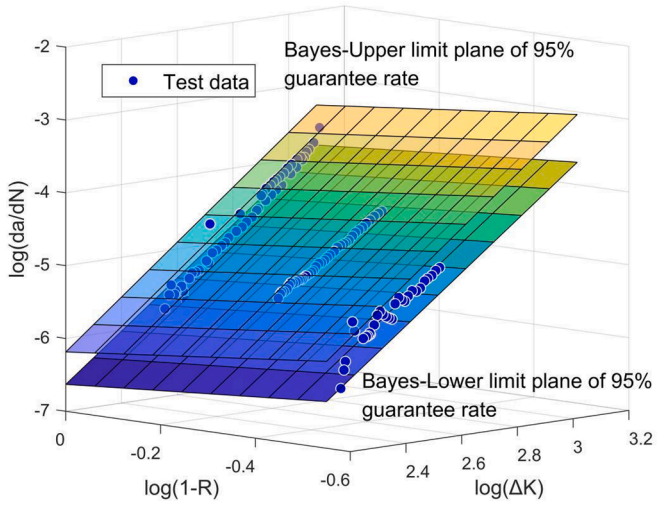

Fig. 9. 95% assurance interval of pure mode I fatigue crack propagation rate.

Table 6
Parameters of Weibull distribution model.

R	C	λ	δ	η
0.1	3.2	28.99	4.61	5.92

2. Determination of material parameters

2.1. Simulation of pure mode I fatigue crack growth

The material properties of S355 steel are listed in Table 1 and Table 2 based on Correia et al [26]. The material coefficient of the Walker equation [25] is obtained based on the test results reported by Dantas [5]. In the test, the compact tensile specimens were carried out under constant amplitude cyclic loads with load ratios of 0.1, 0.5, and 0.7, respectively. The geometric dimensions of the specimens are shown in Fig. 1 and Table 3.

Eqn. (1) and Eqn. (2) shows the Walker equation considering the effect of load ratio effects on fatigue crack propagation rate. After the test data are transferred into logarithmic space, linear fitting was carried out by MATLAB [27] based on the Walker equation. Fig. 2 shows the fitting results of the test data, and Table 4 shows the values of the material coefficient.

$$\frac{da}{dN} = C_0(\overline{\Delta K})^m \tag{1}$$

$$\overline{\Delta K} = \frac{\Delta K}{(1-R)^{1-\gamma}} \tag{2}$$

where:C_0, m, γ are material parameters of the Walker equation.

The pure mode I fatigue crack is simulated by XFEM [23] based on the phantom node method [28] and VCCT [24]. As shown in Fig. 3, in addition to the existing set of nodes, the finite element model also includes a set of virtual nodes at the same position. When the structure has no fatigue failure, the element is complete, and each virtual node is completely constrained to the corresponding real node. When the structure reaches fatigue failure, the element breaks, and the virtual and real nodes cooperate to realize fatigue crack reconstruction. Virtual node and real node are defined by the crack cohesion model [29]. The level set method (LSM) [30] is used to characterize the geometric characteristics of cracks. The modified virtual crack closure method (VCCT) [24] is used to calculate the strain energy release rate G. As shown in Fig. 4, after assuming the material is a linear elastic, the strain energy release rate of pure mode I fatigue crack can be calculated by Eq. (3).

$$G_I = \frac{1}{2}\frac{v_{1,6}F_{v,2,5}}{bd} \tag{3}$$

where: G_I is the Mode I energy release rate; b is the width; d is the length of the elements at the crack front; $F_{v,2,5}$ is the vertical force between nodes 2 and 5; and, $v_{1,6}$ is the vertical displacement between nodes 1 and 6.

To consider the effect of mean stress on fatigue crack propagation rate, the Walker equation [25] is used as the calculation criterion of fatigue crack propagation rate in the numerical model and implemented in the user-defined subroutine 'UMIXMODEFATIGUE'. Finally, the simulation of fatigue crack propagation is realized by commercial software ABAQUS [31]. Fig. 5 shows the flow chart of the subroutine. It is noted that when simulating pure mode-I fatigue crack propagation, the coefficients β and γ in the formula used to calculate the equivalent energy release rate, G_{eq}, in the subroutine are assumed to be equal to 1, which is identical to the authors' previous publication [22]. For the

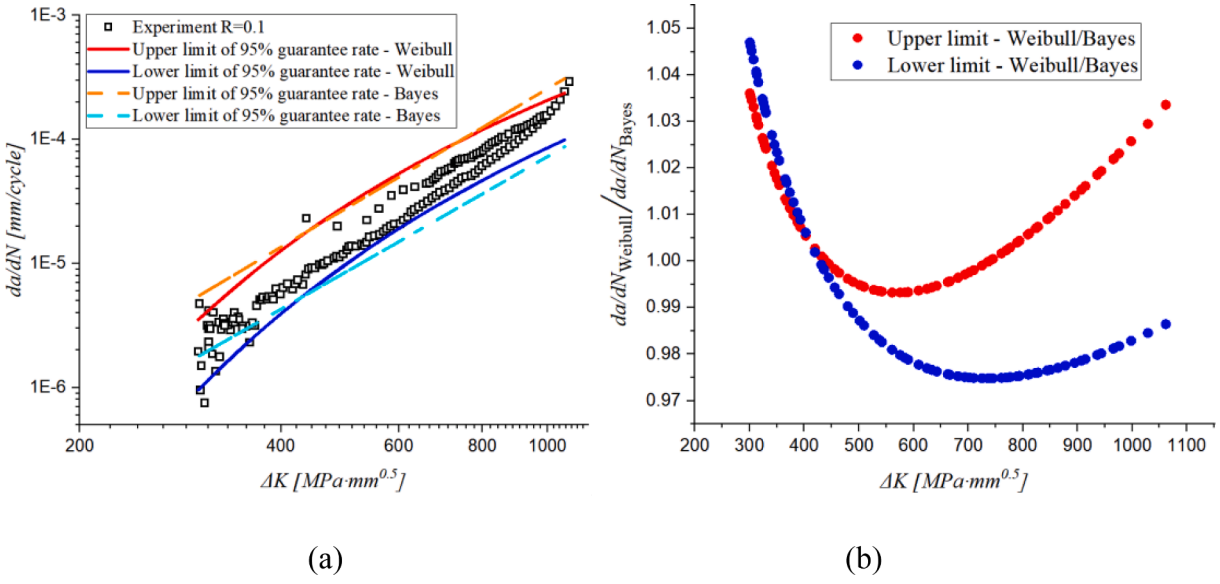

Fig. 10. (a) The probability results of Weibull distribution and Bayes theory, and (b) ratio of fatigue crack propagation rates predicted by two methods.

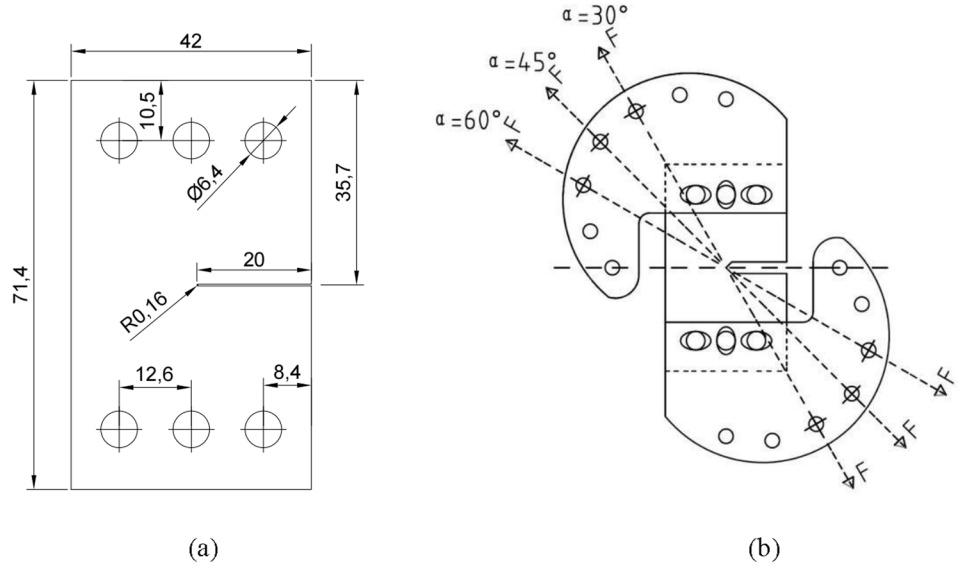

Fig. 11. Compact tension shear specimen and loading set-up [5].

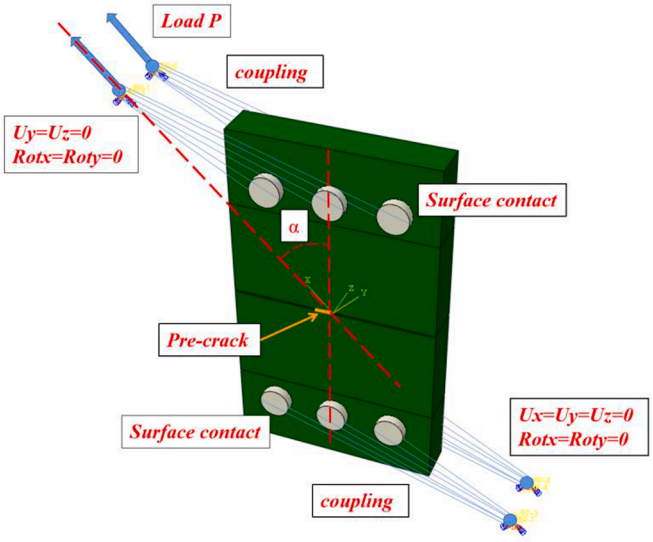

Fig. 12. Boundary conditions of CTS specimen.

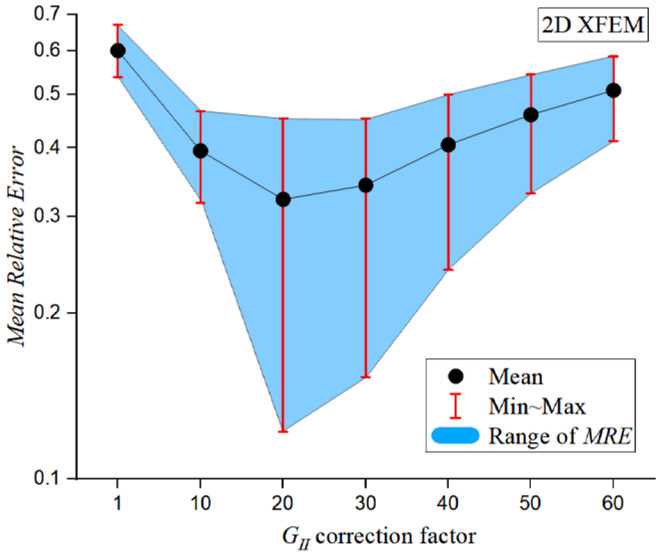

Fig. 13. Influence of G_{II} correction coefficient β on *MRE* of 2D simulation results.

numerical simulation of mixed mode fatigue crack, the coefficients β and γ are obtained by fitting fatigue test data. After obtaining the G_{eq}, the equivalent stress intensity factor range ΔK_{eq} can be obtained according to the fracture mechanics, and then the fatigue crack growth rate da/dN can be calculated.

In this paper, three finite element models are used to simulate pure mode I fatigue crack propagation. The first two are the 2D finite element model with the element type CPE4 (plane strain) and with the element type CPS4 (plane stress), and the last is the three-dimensional finite element model with the element type C3D8. The elastic modulus of the model is defined as equal to 211.6 GPa, the Poisson's ratio of 0.3, the cyclic load with a period of 1 s, and the time increment step is 0.01 s. A rectangular pre-crack was set in the finite element model.

As shown in Fig. 6, the 3D numerical model is constrained by two semi-cylindrical pins based on sensitive analysis in reference [22], two reference points are set at the center of the lower surface of the two pins and coupled with the lower surface of the pin respectively. The lower reference point is fixed, and the upper reference point can only be displaced along the load direction. The pin is in hard contact with the specimen model. The constraints of the 2D numerical model are the same as the 3D numerical model, except for the constraints in the thickness direction. In the numerical simulation, three constant amplitude cyclic loading conditions were considered. For the first condition, the load ratio R is 0.1, and the peak value of fatigue load is 5kN; for the second condition, the load ratio R is 0.5, and the peak value is 8.4 kN; for the third condition, the load ratio R is 0.7, and the peak value is 8.4 kN.

After obtaining the finite element simulation results, the fatigue crack propagation rate is calculated by $\Delta a/\Delta N$. The SIF ranges were computed by Eqn. (4).

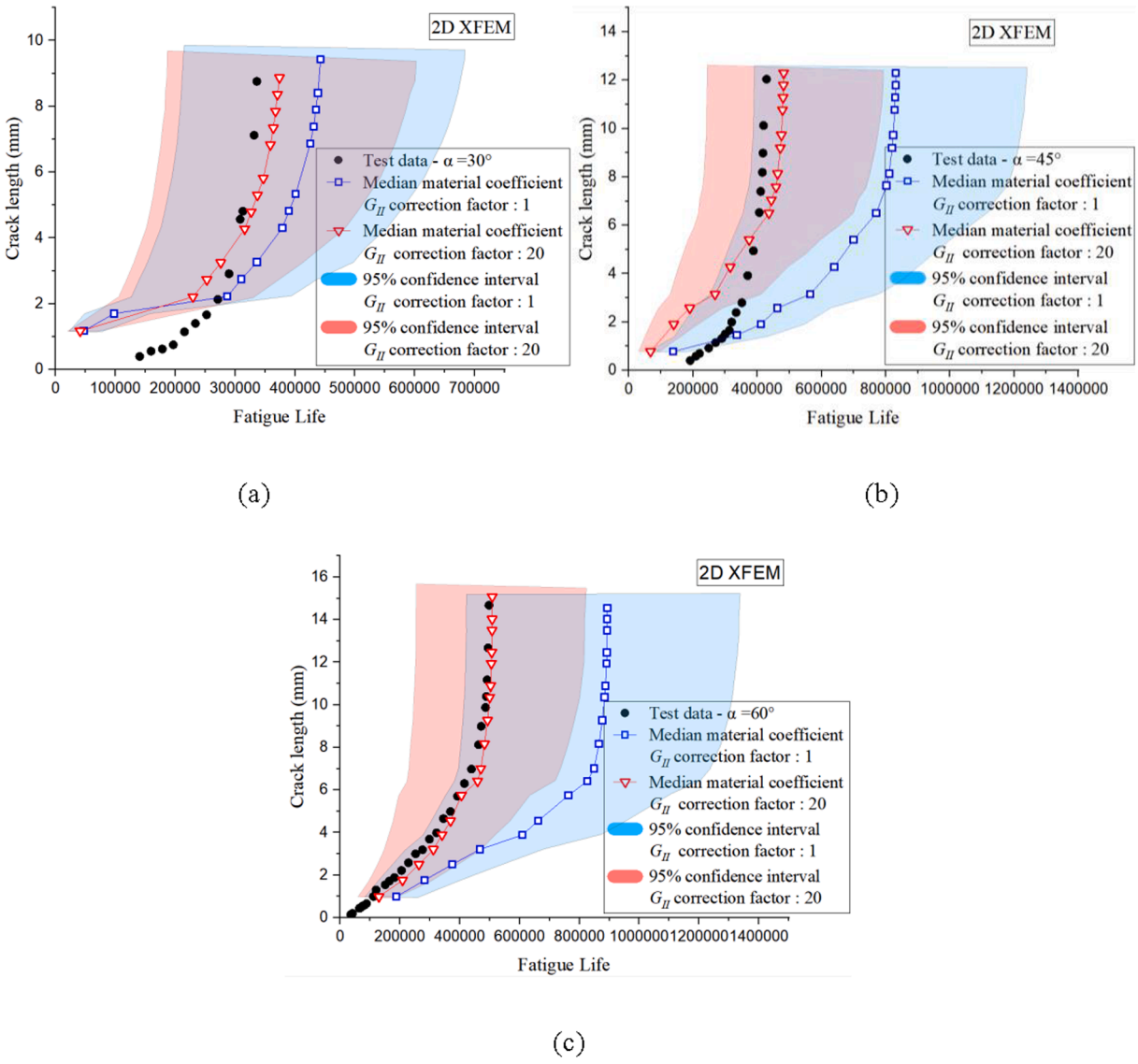

Fig. 14. Comparison between I+II mixed mode fatigue crack propagation simulation results of the 2D numerical model and experimental data.

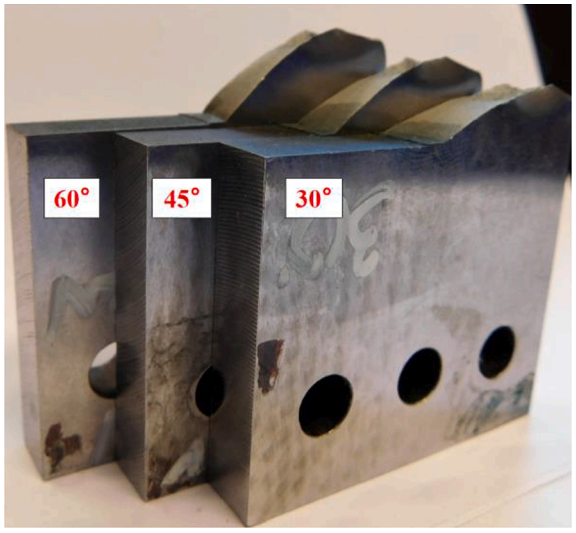

Fig. 15. Failure CTS specimen [5].

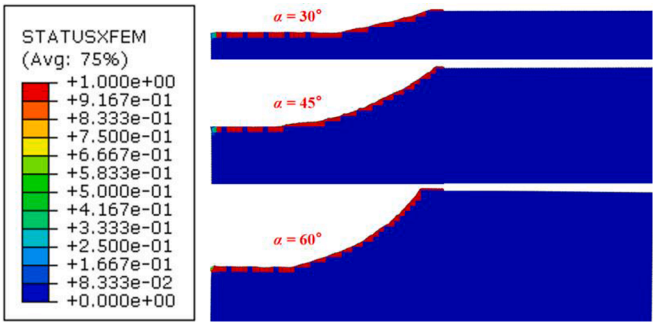

Fig. 16. Fatigue crack propagation path of the 2D numerical model.

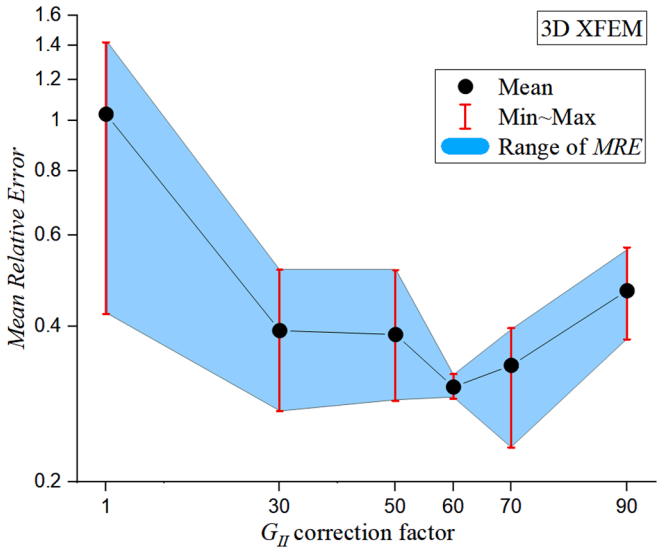

Fig. 17. Influence of G_{II} correction coefficient β on *MRE* of 3D simulation results.

$$\Delta K = \frac{\Delta F(2+\frac{a}{W})(0.886+4.46\frac{a}{W}-13.32(\frac{a}{W})^2+14.72(\frac{a}{W})^3-5.6(\frac{a}{W})^4)}{B\sqrt{W}(1-\frac{a}{W})^{1.5}} \quad (4)$$

Where: ΔF is the applied load range; a is crack size; W is the effective width; and, B is the thickness.

Fig. 7 compares the test data with the simulation results from different finite element models. It should be noted that the fatigue crack propagation rate of the 2D numerical model with element type CPS4 is significantly slower than the test data. The 2D numerical model with element type CPE4 and 3D numerical model agrees well with the experimental data. However, the simulation results of the 3D numerical model are slightly discrete. This may be caused by the slight difference between the rectangular pre-crack in the numerical model and the elliptical pre-crack in reality. Fig. 8 compares the failure mode between numerical simulation and experimental observations where the load ratio is 0.5. A good agreement is observed.

2.2. Probabilistic analysis of fatigue crack propagation rate

Due to the fatigue test being very sensitive to micro defects of materials, the scatter of fatigue crack propagation test results is relatively larger than general static test results. To study fatigue performance more comprehensively, the probability analysis of the test data is carried out in this section. The Bayesian method based on Markov chain Monte Carlo (MCMC) is employed to sample the probability distribution. The detailed procedures can refer to [32].

Table 5 shows the walker equation material parameters with 95 % assurance, and Fig. 9 shows the fatigue crack propagation rate plane with 95 % assurance. In addition, Weibull distribution is used to validate the probabilistic results from the MCMC method. Noted that the load ratio is fixed when using the analytical Weibull model based on Profatigue software [33]. Eqn. (5) and (6) give a three-parameter model of Paris law.

$$P_f(dN/da,\Delta K) = 1-exp\left\{-(\frac{(logdN/da-B)(log\Delta K-C)-\lambda}{\delta})^{\eta}\right\} \quad (5)$$

$$(logdN/da-B)(log\Delta K-C) > \lambda \quad (6)$$

where: P_f is the probability of failure for a specimen; N is the number of cycles to failure; B and C are the threshold values; λ, δ, and η are the location, scale, and shape non-dimensional parameters of the Weibull model, respectively.

Table 6 shows the material coefficients of the Weibull model. It is noted that the influence of the load ratio cannot be considered in Eq. (5), so the load ratio is fixed as 0.1 for the validation. Fig. 10 (a) showed the prediction results of the two probability methods. The Y axial in Fig. 10 (b) represents the fatigue crack propagation rate predicted by the Weibull distribution divided by the rate predicted by the Bayesian method. It is noted that the maximum error of the two probability methods is less than 5 %. It represents that the material coefficient of the Walker equation with 95 % guarantee rate calculated by the Bayesian method is correct. The median material coefficient of the Walker equation shown in Table 4 and the material coefficient with a 95 % guarantee rate shown in Table 5 will be used in the mixed fatigue crack growth analysis.

3. Fatigue crack propagation under I+II loading conditions

3.1. Finite element model of I+II mixed mode fatigue crack propagation

The I + II mixed mode fatigue crack propagation test data reported by Dantas [5] were used to fit the proposed coefficients β (The role of coefficient β in numerical simulation is shown in Fig. 5). A constant amplitude cyclic load with a load ratio of 0.1 is applied to the compact tension shear specimen (CTS), and the peak value of the fatigue load is 7.5kN. The geometric dimensions of the specimen are shown in Fig. 11 (a). The cyclic load is applied through the load set-up shown in Fig. 11 (b). There are seven holes on the outer edge of the load set-up, which allows the test to be carried out with different load angles. For $\alpha = 0°$, the test is performed under pure mode I, while for $\alpha = 90°$ is obtained under pure mode II loading conditions. The tests were carried out under the loading conditions with loading angles of 30°, 45°, and 60°. Fatigue crack propagation tests were carried out on a total of three specimens.

In this section, the 2D numerical model with element type CPE4 and the 3D numerical model with element type C3D8 are used to simulate mixed-mode fatigue cracks, respectively. For 2D finite element models, the tests are simulated under the conditions that β is equal to 1, 10, 20, 30, 40, 50 and 60, respectively, and, for 3D finite element models, the tests are simulated under the conditions that β is equal to 1, 30, 50, 60, 70 and 90, respectively. It is noted that the value of β obtained by trial calculation of the finite element model.

Fig. 12 shows the loading conditions of the 3D model. Six cylindrical rigid steel bars are used to model the loading test set-up. The two ends of the three rigid steel bars are coupled by reference points. The position of the reference point is determined based on CTS tests. The cyclic load is applied to the upper reference point. All the degrees of freedom are fixed for the lower reference point, and two displacement degrees of freedom in the horizontal direction and out-of-plane direction, as well as its two rotational degrees of freedom out-of-plane, are fixed for the upper reference point. A rectangular pre-crack was set at the notch of the finite element model. The 2D finite element model has the same constraints as the 3D finite element model except thickness direction is neglected.

3.2. Comparisons between simulation results and test data

3.2.1. Comparison between simulation results of the 2D numerical model and experimental data

To determine the value of the coefficient β, the Mean Relative Error (*MRE*) between the numerical simulation results using the median material coefficient of the Walker equation and the experimental data was calculated according to Eqn. (7). Since the test is conducted at three loading angles, three *MRE* values can be calculated for a value of β, and the maximum, minimum and mean values of the three *MRE* are given in Fig. 13. It is noted that for the 2D numerical model, when β is equal to 20, the simulation results are most consistent with the experimental data.

$$MRE = \frac{1}{n}\sum_{i=1}^{n}|\mu_i-\mu_i'|/\mu_i \quad (7)$$

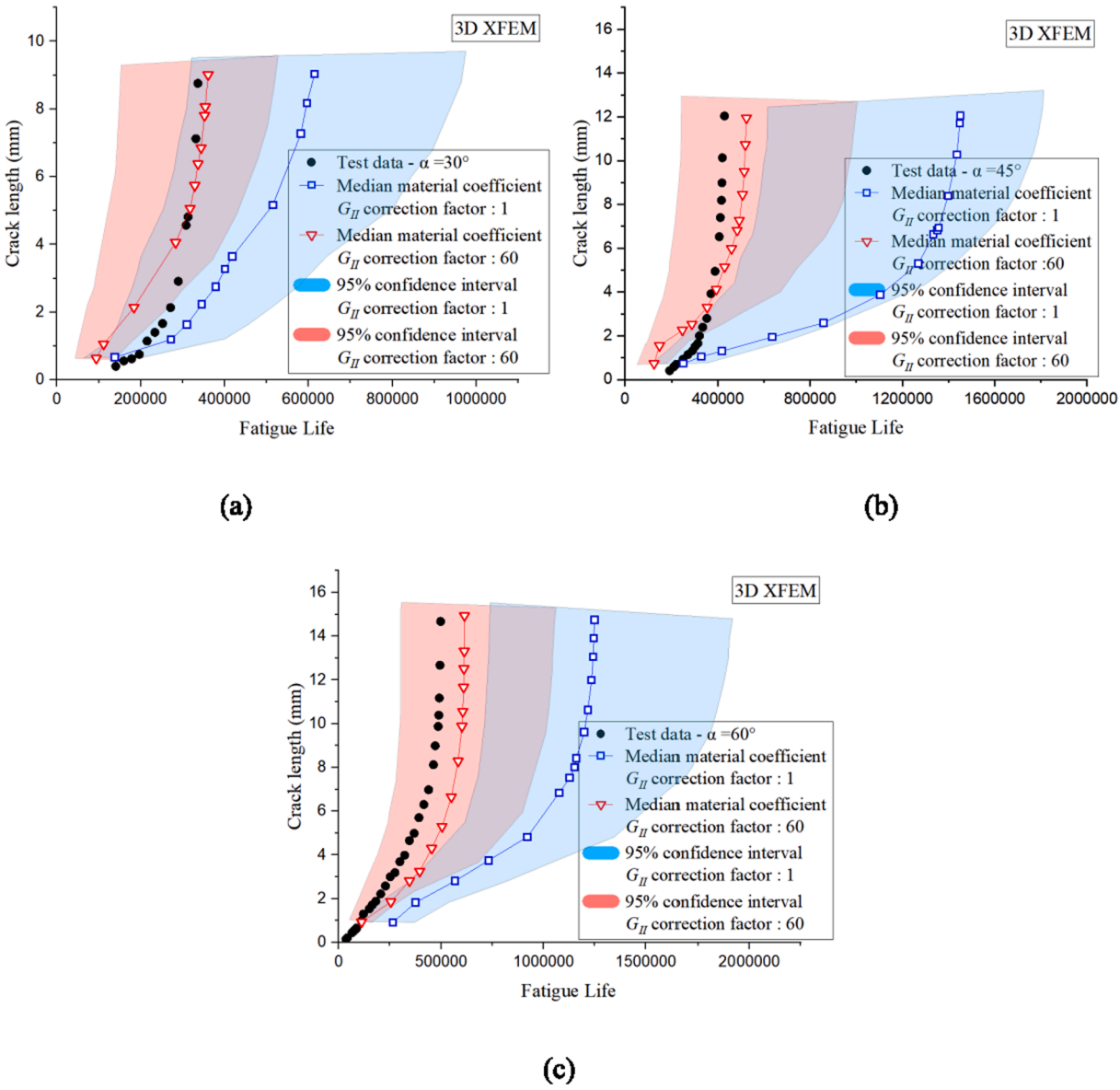

Fig. 18. Comparison between I+II mixed mode fatigue crack propagation simulation results of the 3D numerical model and experimental data.

where μ_i and μ_i' are the number of load cycles corresponding to the fatigue crack propagation length of the test data and simulation results, respectively. The value of n is the number of test points.

In Fig. 14, the simulation results with β equal to 1 and 20 are compared with the test data. In order to consider the scatter of the test results, the coefficient with a 95 % guarantee rate of the Walker equation [25] is used to predict the fatigue crack propagation, and the comparisons with β equal to 1 and 20 are shown in Fig. 14. Obviously, the test data do not fall into the guarantee rate range at all and there is a big gap between the simulation results of the three loading angles and the test data when the coefficient β of the G_{II} is equal to 1. When the β is equal to 20, the simulation results with a loading angle of 60° are most consistent with the experimental data. However, in the simulation results with loading angles of 30° and 45°, the fatigue crack propagation length at the initial stage is much larger than the test data. This may be caused by not considering the short crack closure effect in the numerical model.

Fig. 15 shows the experimental fractured patter of specimen exposed to I + II mixed loading. The fatigue crack propagation path becomes steep with the increase of loading angle. Fig. 16 shows the simulated fatigue crack propagation path under different loading angles in terms of the 2D model. The fatigue failure pattern agreed well.

3.2.2. *Comparison between simulation results of 3D numerical model and experimental data*

In Fig. 17, the simulation results of the 3D numerical model were compared with the experimental data, and the *MRE* value was calculated. When the correction coefficient β before G_{II} is equal to 60, the mean value of *MRE* calculated by the simulation results, and the test data reaches the minimum, that is, the simulation results are most consistent with the test data. When the mean value of *MRE* reaches the minimum, it does not mean that the *MRE* corresponding to the simulation results under the three loading shear angles all reaches the minimum. When the correction coefficient β is equal to 70, the simulation results with a loading shear angle of 60° fit the test data best, but the *MRE* mean value at this time is bigger than the *MRE* mean value when

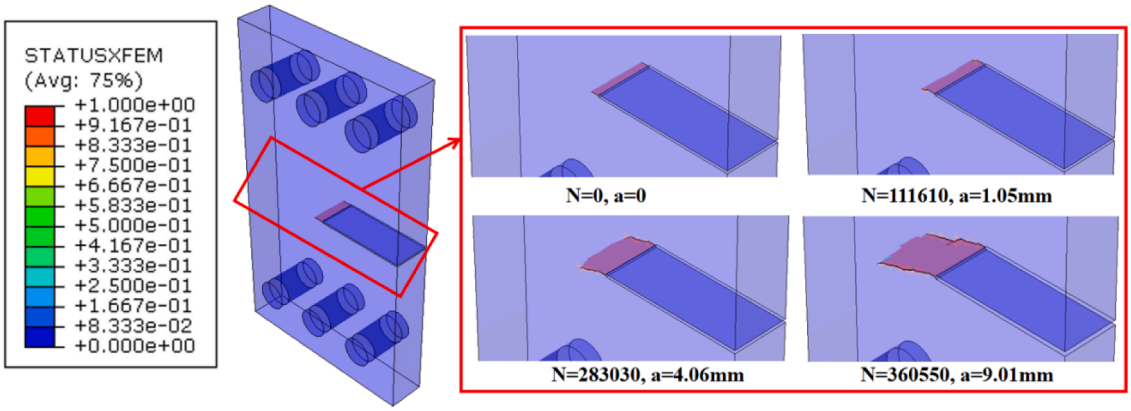

(a) 30 degree loading condition

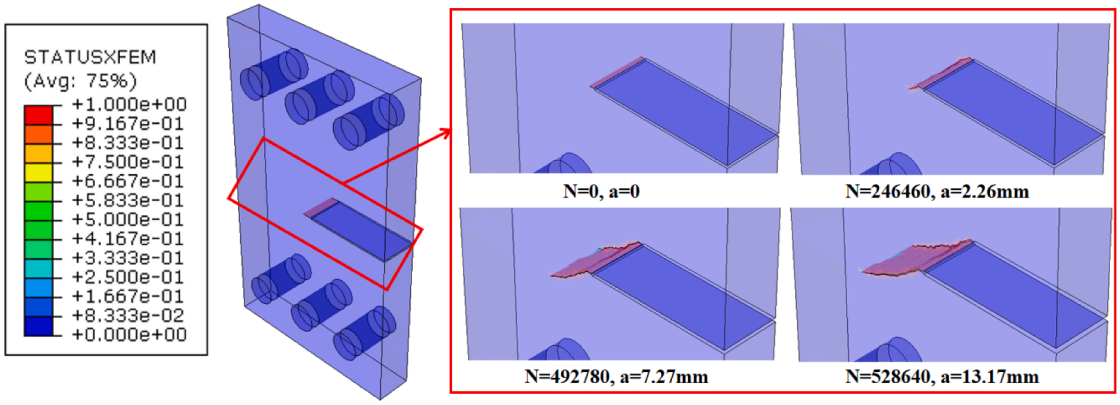

(b) 45-degree loading condition

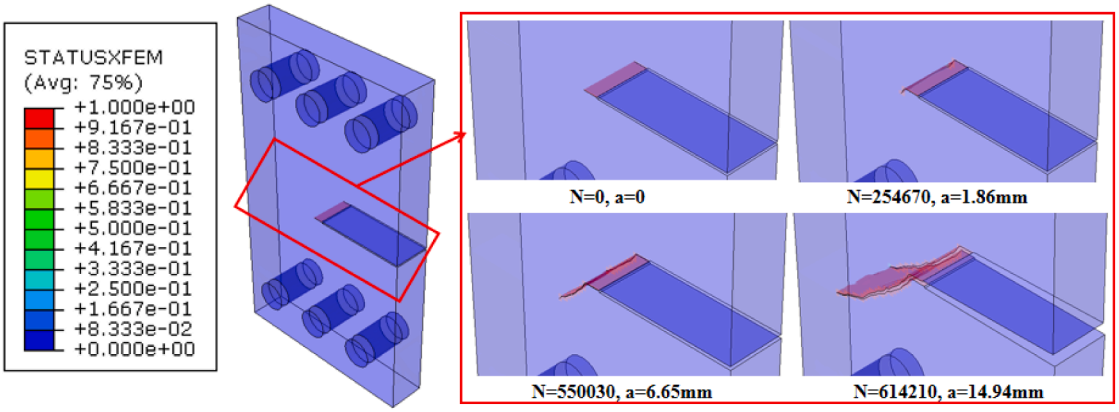

(c) 60-degree loading condition

Fig. 19. I + II Mixed mode fatigue crack propagation.

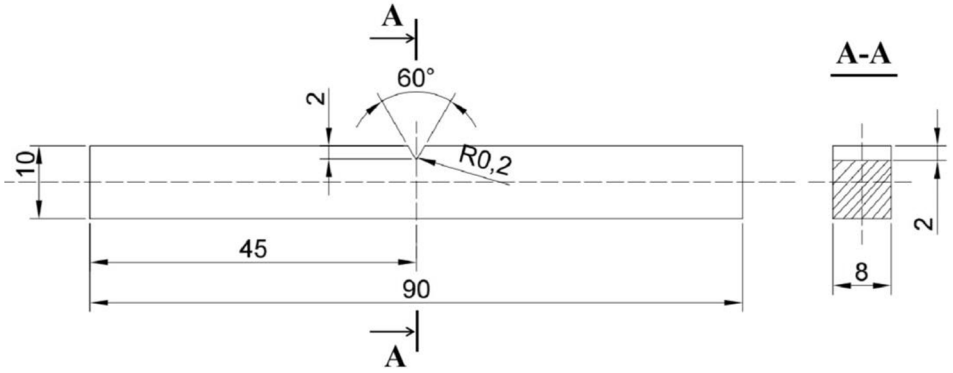

Fig. 20. I + III mixed mode fatigue specimen [6].

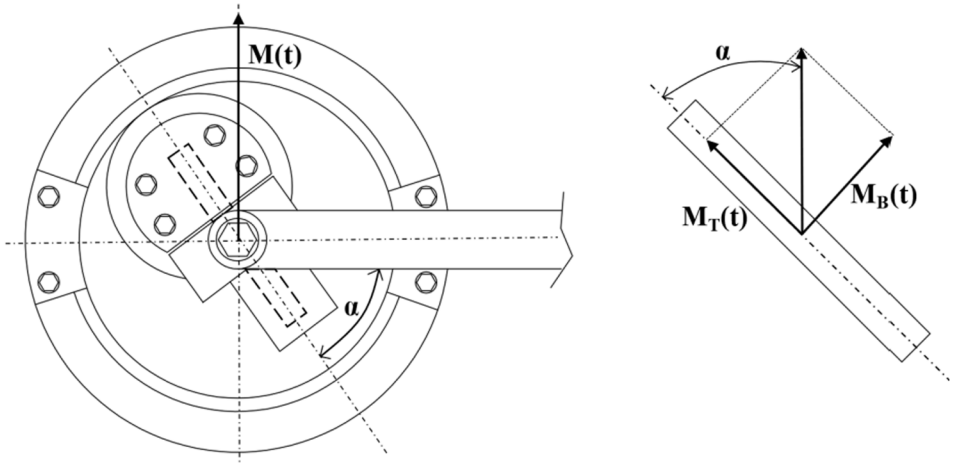

Fig. 21. I + III mixed mode fatigue crack propagation test loading conditions [6].

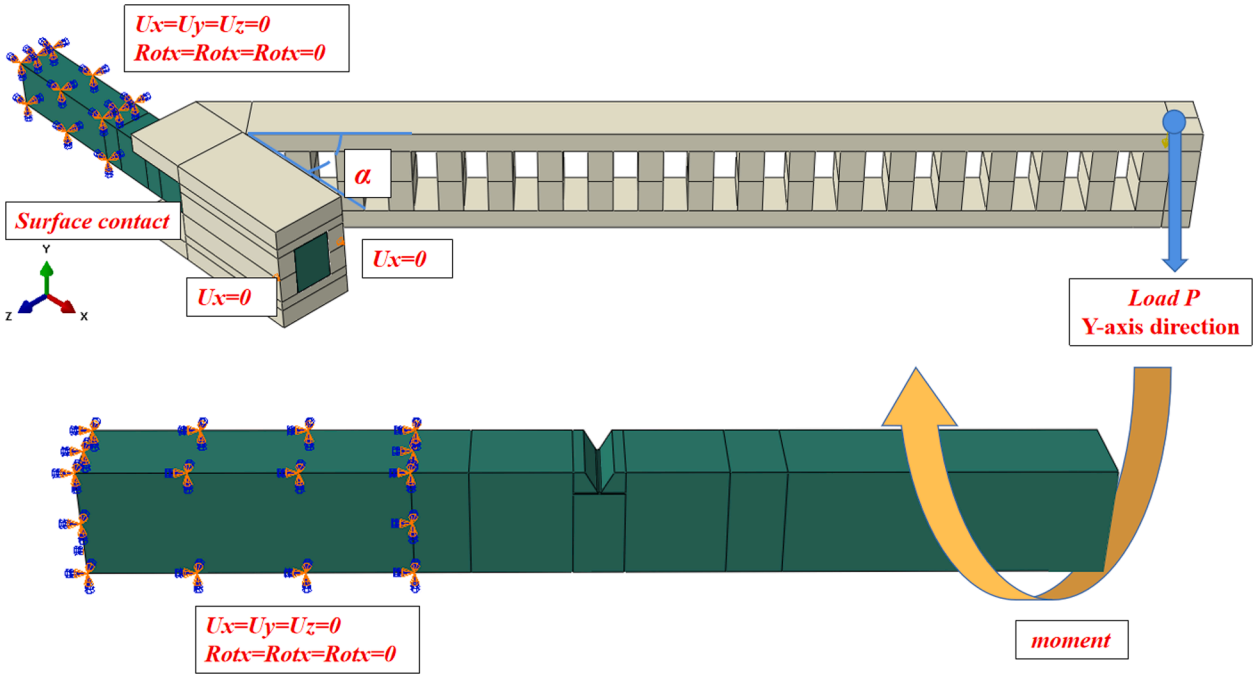

Fig. 22. Boundary conditions of I + III mixed mode fatigue specimen.

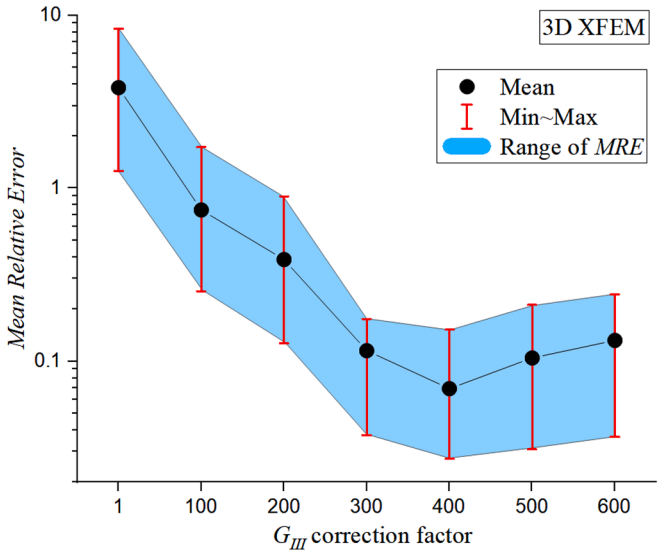

Fig. 23. Influence of G_{III} correction coefficient γ on *MRE* of 3D simulation results.

the correction coefficient β is 60.

In Fig. 18, the simulation results with β equal to 1 and 60 are compared with the test results. When the correction factor β is equal to 60, the initial fatigue crack propagation length of the finite element simulation results with loading angles of 30° and 45° is slightly larger than the test data, so that the test data does not fall into the guarantee rate range at the initial stage. The simulation results with a load angle of 60° are in good agreement with the test data, and all the test data fall into the guarantee rate range. On the whole, for the 3D numerical model, after modifying the coefficient β before G_{II}, the accuracy of fatigue crack propagation exposed to mixed mode agreed much better.

Fig. 19 shows the fatigue propagation process exposed to I + II mixed mode with β value of 60. It is easy to see that the propagation path of fatigue crack becomes steep with the increase of loading shear angle. The fatigue failure pattern also agreed well when compared to experimental observations in Fig. 15.

4. Fatigue crack propagation under I+III loading conditions

4.1. Finite element model of I+III mixed mode fatigue crack propagation

In this chapter, to explore the properties of I + III mixed mode fatigue cracks, the test data of Rozumek et al. [6] are analyzed. It is noted that the steel used in the fatigue crack propagation test study in this paper by Rozumek et al. [6] and Dantas [5] is the same batch. The geometric dimensions of the specimen are shown in Fig. 20. As shown in Fig. 21, in the test, the specimen is subjected to constant amplitude cyclic moment with load ratio R = 0, and the cyclic moment is realized through the constant amplitude cyclic load at the end of loading arm. The peak value of the fatigue load is 17.19 N • m. The cyclic moment can be divided into a bending moment M_B and torsional moment M_T, The ratio of M_T to M_B can be changed by changing the angle α between the loading arm and the specimen. There are three loading angles in the test, that is α = 30°, 45°, and 60°. Fatigue crack propagation tests were carried out on a total of three specimens. In fact, the specimen is also subjected to a shear force, but it is ignored because it is much less than the the stress coming from bending and torsional moment [6].

In the fatigue crack propagation process when the specimen is exposed to I + III mixed mode loading, the coefficient β is assumed to be 60, and the coefficient γ is fitted by the parametric analysis against experimental results (The role of coefficients β and γ in numerical simulation is shown in Fig. 5). Mode III does not exist for the 2D model, only the 3D model is used to simulate fatigue crack propagation. The 3D model is used to simulate the fatigue crack propagation under the condition that γ is equal to 1, 100, 200, 300, 400, 500, and 600. Fig. 22 showed the boundary conditions of the numerical model. One end of the model is fixed, and the other end is connected by the loading arm. General contact with "hard" normal properties is defined between the specimen and the loading arm. A displacement constraint along the axial direction of the specimen is set at the rear end of the loading arm to prevent sliding, and a constant amplitude cyclic load is applied at the far end of the loading arm.

4.2. Comparisons between simulation results and test data

Fig. 23 shows the *MRE* value between the simulation results and the test data. When the coefficient γ before the term G_{III} is equal to 400, the simulation results are most consistent with the experimental data. It should be noted that no pre-crack was carried out on the test specimen, so the numerical simulation began after the fatigue crack of the test specimen extended for a certain length. Fig. 24 shows the comparison between the experimental data and the numerical simulation results when γ is equal to 1 and 400. The simulation results for loading angles α = 30° and 45° are in good agreement with the experimental data. However, the simulation results of loading angle α = 60° are inconsistent with the test data, and the test data do not fall into the guarantee rate range, which may be caused by the scattering of the test data.

Fig. 25 shows the fatigue crack propagation process under I + III mixed-mode in the finite element simulation results when γ is equal to 400. The fatigue cracks gradually extended into a torsional surface, and the fatigue propagation surface becomes more and more distorted with the increase of loading angle α.

5. Verification of correction coefficients

In this paper, I + II and I + III mixed mode fatigue crack propagation are successfully simulated by modifying the coefficients β and γ before G_{II} and G_{III} in the calculation formula of G_{eq}. The effects of the revised coefficient on pure mode I fatigue crack growth were checked by comparing the test data with the simulation results again. It is noted that the load and boundary conditions of the numerical model are consistent with the model in Section 2.1.

Hence, β and γ are assumed to be 60 and 400, respectively. The simulation results are shown in Fig. 26. Although the simulation results under the three load ratios deviate slightly from the test data, they fall into the guarantee rate range, which proves that through the correction of the coefficient before G_{II} and G_{III} in the formula of G_{eq}, the extended finite element method is still valid for the pure mode I fatigue crack propagation.

6. Conclusions

This paper is the continuation of the authors' previous publication [22]. In this paper, two modification coefficients before G_{II} and G_{III} of the formula to calculate the equivalent energy release rate, G_{eq}, are introduced, to better calculate the equivalent energy release rate exposed to mixed-mode loading. The following conclusions are drawn:

(1) The probability analysis of pure mode I test data is carried out by the Bayesian method. Based on the Walker equation, the 95 % assurance interval of fatigue crack propagation rate is obtained. The probability results are validated by Weibull distribution with a fixed loading ratio. Because the error of the two methods is less than 5 %, the practicability of the Bayesian method in predicting fatigue crack propagation rate is proved.

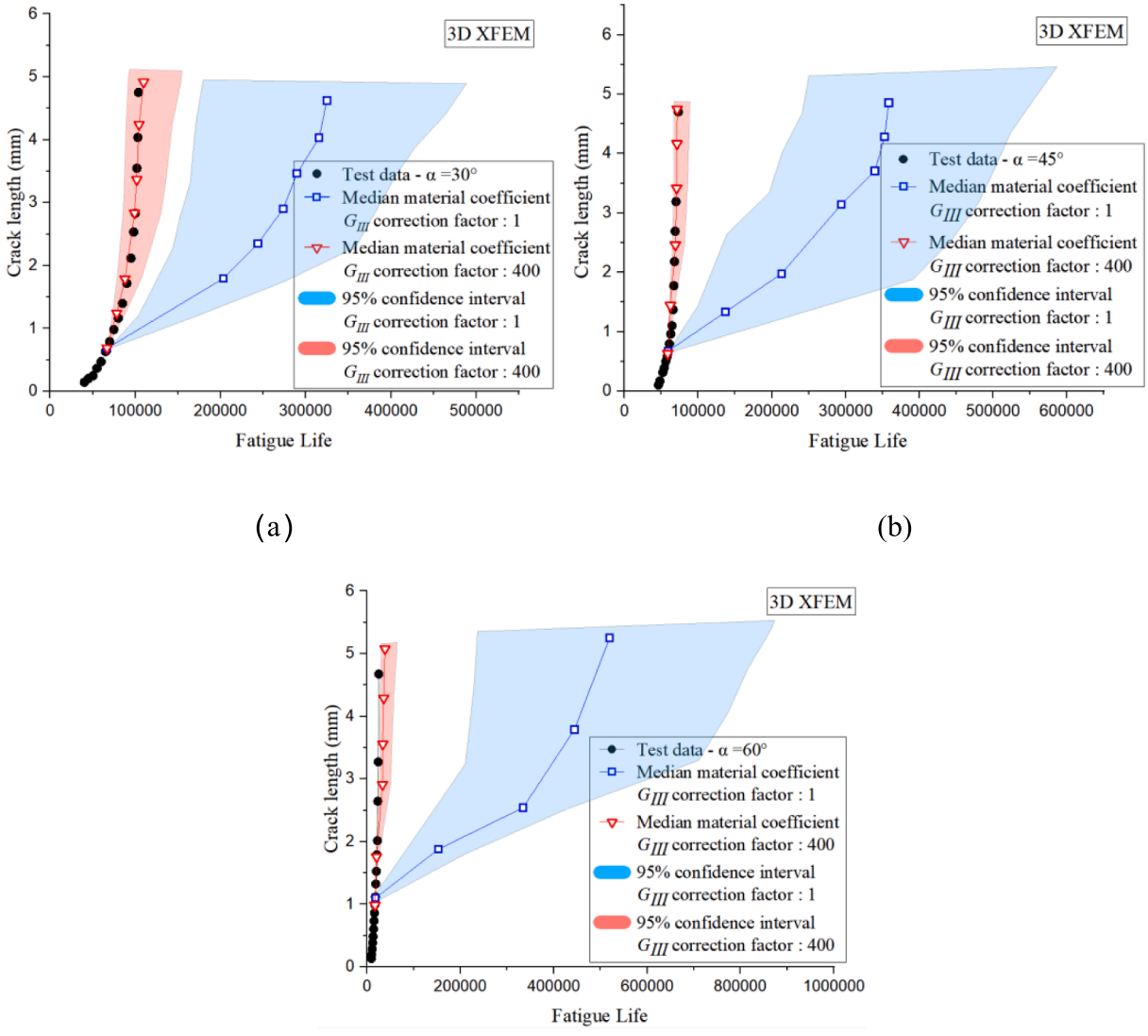

Fig. 24. Comparison between I+III mixed mode fatigue crack propagation simulation results of the 3D numerical model and experimental data.

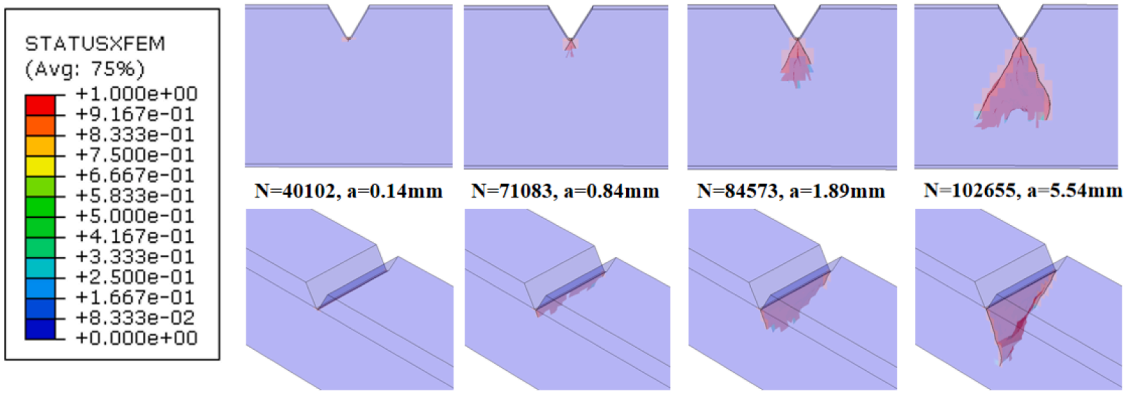

(a) 30 degree loading condition

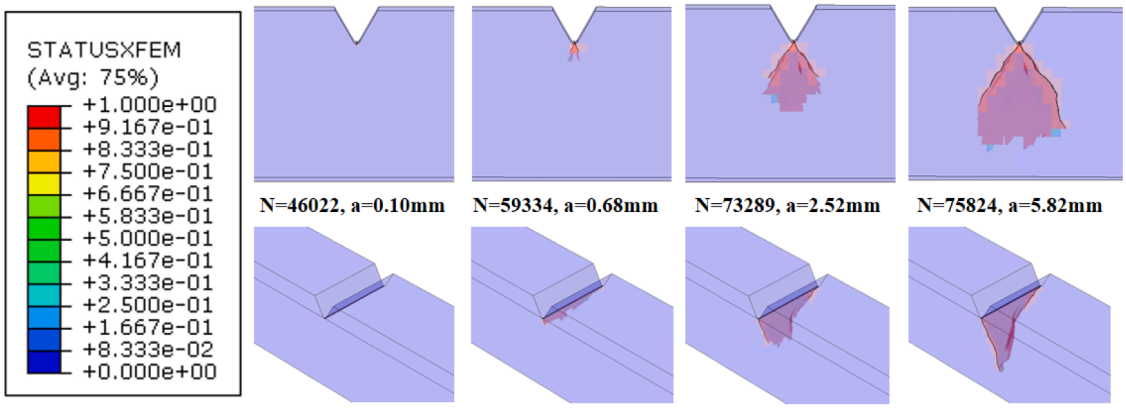

(b) 45-degree loading condition

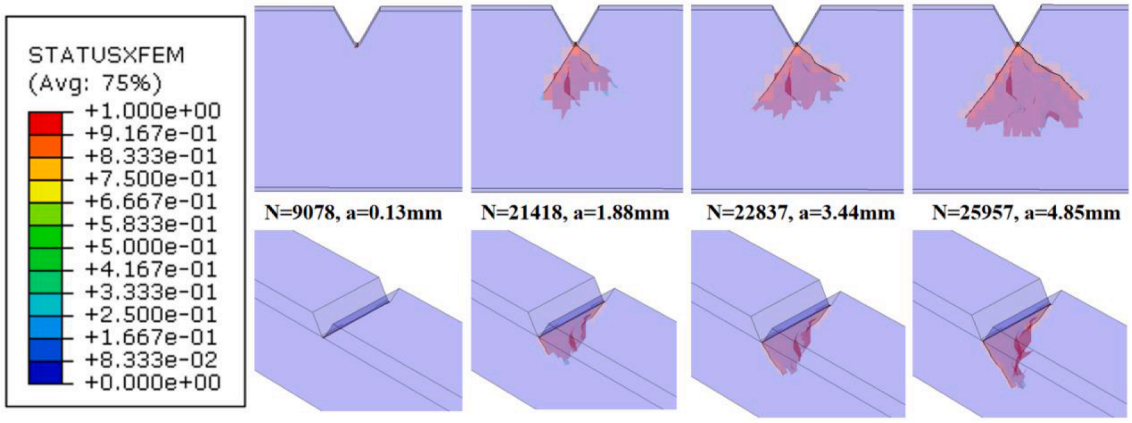

(c) 60-degree loading condition

Fig. 25. I + III mixed mode fatigue crack propagation.

(2) By modifying the coefficients before G_{II} and G_{III} in the formula of G_{eq}, the I+II and I+III mixed mode fatigue crack can be successfully simulated based on XFEM and VCCT methods using a 3D numerical model. According to the simulation results, when the coefficient of G_{II}, β, is equal to 60, and, the coefficient of G_{III}, γ, is equal to 400, the simulation results are most consistent with the experimental data.

(3) The 2D numerical model with element type CPE4 can accurately simulate the pure mode I fatigue crack propagation, while the fatigue crack propagation rate of the 2D numerical model with element type CPS4 is less than the test data. When the 2D numerical model is used to simulate the mixed mode I + II fatigue crack, the initial crack propagation length of the simulation results with shear angles of 30° and 45° is much larger than the test data.

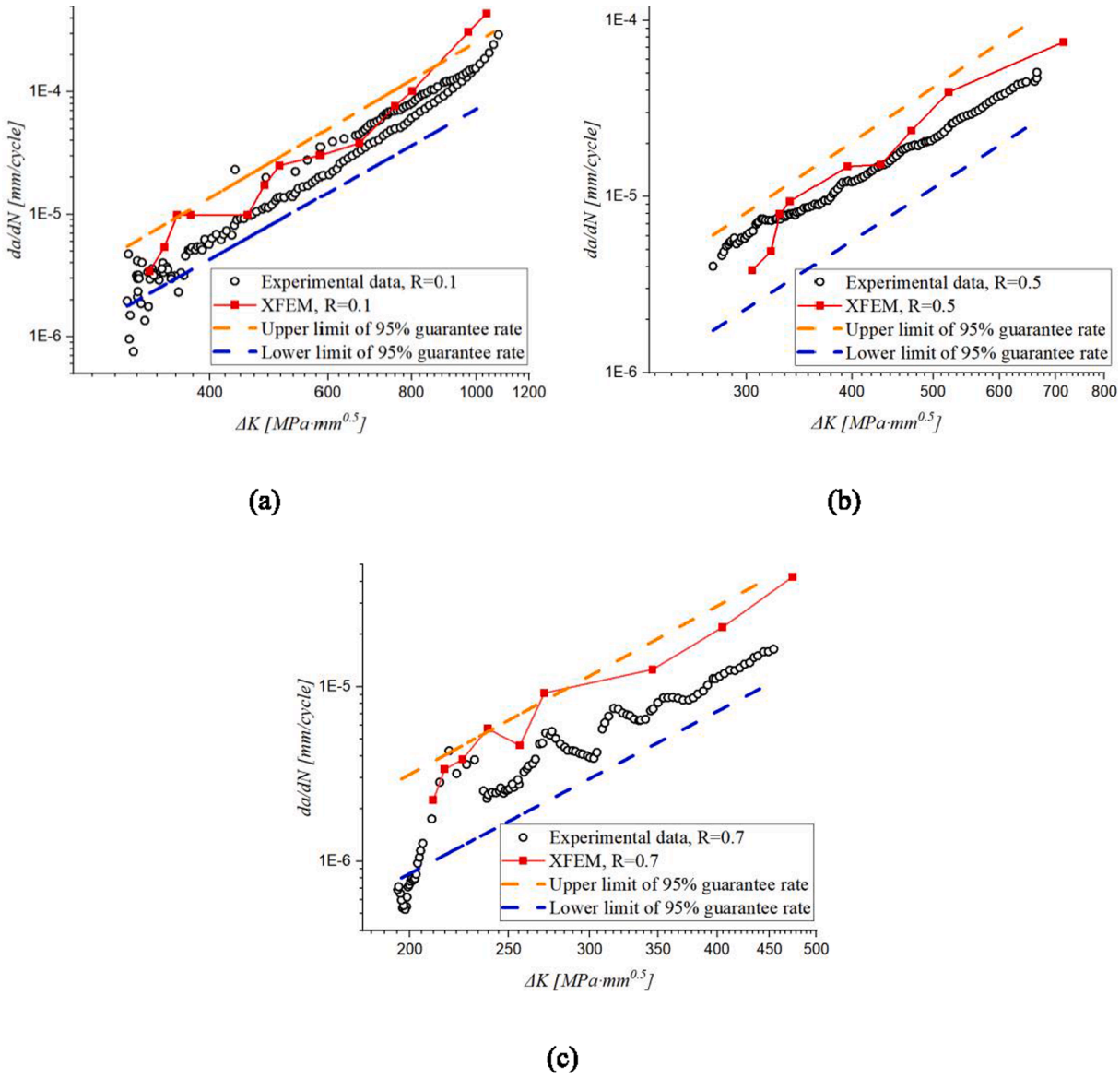

Fig. 26. Simulation results of pure mode I fatigue crack considering two correction coefficients.

CRediT authorship contribution statement

Haohui Xin: Formal analysis, Validation, Writing – review & editing. **Jielin Liu:** Conceptualization, Writing – original draft. **José A.F.O. Correia:** Formal analysis, Writing – original draft. **Filippo Berto:** Writing – review & editing. **Milan Veljkovic:** Writing – review & editing. **Guian Qian:** Writing – review & editing.

Declaration of Competing Interest

The authors declare that they have no known competing financial interests or personal relationships that could have appeared to influence the work reported in this paper.

Data availability

Data will be made available on request.

Acknowledgments

The author Haohui Xin gratefully acknowledges the financial support provided by the high-level innovation and Entrepreneurship Talent Project from QinChuangyuan (Grants #2021QCYRC4-32) of Shaanxi Province of the People's Republic of China. The author José A.F.O. Correia would like to acknowledge the support given by: base funding - UIDB/04708/2020 and programmatic funding - UIDP/04708/2020 of the CONSTRUCT - Instituto de I&D em Estruturas e Construções - funded by national funds through the FCT/MCTES (PIDDAC); project grant - POCI-01-0145-FEDER-030103 (FiberBridge - Fatigue strengthening and assessment of railway metallic bridges using fiber-reinforced polymers) by FEDER funds through COMPETE2020 (POCI) and by national funds (PIDDAC) through the Portuguese Science Foundation (FCT/MCTES). Additionally, this work is financially supported by national funds through the FCT/MCTES (PIDDAC), under the MIT Portugal Program under the project MIT-EXPL/SOE/0054/2021.

References

[1] A. Mohabeddine, J.A.F.O. Correia, P.A. Montenegro, J.M. Castro, Fatigue crack growth modelling for cracked small-scale structural details repaired with CFRP, Thin-Walled Struct. 161 (2021) 107525.
[2] H.T. Wang, G. Wu, Crack propagation prediction of double-edged cracked steel beams strengthened with FRP plates, Thin-Walled Struct. 127 (2018) 459–468.

[3] Q.Q. Yu, X.L. Zhao, T. Chen, X.L. Gu, Z.G. Xiao, Crack propagation prediction of CFRP retrofitted steel plates with different degrees of damage using BEM, Thin-Walled Struct. 82 (2014) 145–158.
[4] S.-P. Zhu, W.-L. Ye, J.A.F.O. Correia, A.M.P. Jesus, Q. Wang, Stress gradient effect in metal fatigue: Review and solutions, Theor. Appl. Fract. Mech. 121 (2022) 103513.
[5] R.G.R. Dantas, Fatigue life estimation of steel half-pipes bolted connections for onshore wind towers applications, MSc. Thesis, University of Porto, 2019, 183 pages.
[6] D. Rozumek, Z. Marciniak, G. Lesiuk, J.A. Correia, A.M. de Jesus, Experimental and numerical investigation of mixed mode I+ II and I+ III fatigue crack growth in S355J0 steel, Int. J. Fatigue 113 (2018) 160–170.
[7] K. Rege, J. Grønsund, D.G. Pavlou, Mixed-mode I and II fatigue crack growth retardation due to overload: An experimental study, Int. J. Fatigue 129 (2019) 105227.
[8] B. Pedrosa, J. Correia, G. Lesiuk, C. Rebelo, M. Veljkovic, Fatigue crack growth modelling for S355 structural steel considering plasticity-induced crack-closure by means of UniGrow model, Int. J. Fatigue 164 (2022) 107120.
[9] S. Sajith, K.S.R.K. Murthy, P.S. Robi, Experimental and numerical investigation of mixed mode fatigue crack growth models in aluminum 6061–T6, Int. J. Fatigue 130 (2020) 105285.
[10] G. Lesiuk, M. Smolnicki, R. Mech, A. Zięty, C. Fragassa, Analysis of fatigue crack growth under mixed mode (I+ II) loading conditions in rail steel using CTS specimen, Eng. Fail. Anal. 109 (2020), 104354.
[11] S. Qi, L.X. Cai, C. Bao, K.K. Shi, H.L. Wu, The prediction models for fatigue crack propagation rates of mixed-mode I-II cracks, Eng. Fract. Mech. 205 (2019) 218–228.
[12] S. Qi, L.X. Cai, C. Bao, H. Chen, K.K. Shi, H.L. Wu, Analytical theory for fatigue crack propagation rates of mixed-mode I-II cracks and its application, Int. J. Fatigue 119 (2019) 150–159.
[13] S.P. Zhu, Y.Z. Hao, D. Liao, Probabilistic modeling and simulation of multiple surface crack propagation and coalescence, App. Math. Model. 78 (2020) 383–398.
[14] T. Chen, L. Li, N. Zhang, X. Song, Y. Hidekuma, Fatigue performance test on inclined central cracked steel plates repaired with CFRP strand sheets, Thin-Walled Struct. 130 (2018) 414–423.
[15] I. Barsoum, H. Almansoori, A.A. Almazrouei, E. Gunister, Fracture mechanics testing and crack propagation modelling in polypropylene pipes, Int. J. Struct. Integrity 12 (2) (2020) 271–283.
[16] D.G. Pavlou, G.N. Labeas, N.V. Vlachakis, F.G. Pavlou, Fatigue crack propagation trajectories under mixed-mode cyclic loading, Eng. Struct. 25 (7) (2003) 869–875.
[17] Y. Yu, B. Kurian, W. Zhang, C.S. Cai, Y. Liu, Fatigue damage prognosis of steel bridges under traffic loading using a time-based crack growth method, Eng. Struct. 237 (2021) 112162.
[18] J. Heng, Z. Zhou, Y. Zou, S. Kaewunruen, GPR-assisted evaluation of probabilistic fatigue crack growth in rib-to-deck joints in orthotropic steel decks considering mixed failure models, Eng. Struct. 252 (2022) 113688.
[19] L. Li, T. Chen, N. Zhang, Numerical analysis of fatigue performance of CFRP–repaired steel plates with central inclined cracks, Eng. Struct. 185 (2019) 194–202.
[20] C. Huang, T. Chen, S. Feng, Finite element analysis of fatigue crack growth in CFRP-repaired four-point bend specimens, Eng. Struct. 183 (2019) 398–407.
[21] N.J. Aljabar, X.L. Zhao, R. Al-Mahaidi, E. Ghafoori, M. Motavalli, Y.C. Koay, Experimental investigation on the CFRP strengthening efficiency of steel plates with inclined cracks under fatigue loading, Eng. Struct. 172 (2018) 877–890.
[22] H. Xin, J.A.F.O. Correia, M. Veljkovic, Three-dimensional fatigue crack propagation simulation using extended finite element methods for steel grades S355 and S690 considering mean stress effects, Eng. Struct. 227 (2021) 111414.
[23] G. Zi, T. Belytschko, New crack-tip elements for XFEM and applications to cohesive cracks, Int. J. Numer. Meth. Eng. 57 (15) (2003) 2221–2240.
[24] L.R. Deobald, G.E. Mabson, S. Engelstad, M. Prabhakar, M. Gurvich, W. Seneviratne, ... & R. Krueger, Guidelines for VCCT-based interlaminar fatigue and progressive failure finite element analysis (No. NASA/TM-2017-219663), 2017.
[25] K. Walker, The effect of stress ratio during crack propagation and fatigue for 2024–T3 and 7075–T6 aluminum. Effects of Environment and Complex Load History on Fatigue Life, ASTM International, 1970, pp. 1–14.
[26] J.A.F.O. Correia, A.M.P. de Jesus, A.C. Fernández Canteli, R.A.B. Calçada, Modelling probabilistic fatigue crack propagation rates for a mild structural steel, Frattura ed Integrita Strutturale 31 (2015) 80–96.
[27] D.J. Higham, N.J. Higham, MATLAB Guide: Society for Industrial and Applied Mathematics, 2000.
[28] T. Rabczuk, G. Zi, A. Gerstenberger, W.A. Wall, A new crack tip element for the phantom-node method with arbitrary cohesive cracks, Int. J. Numer. Meth. Eng. 75 (5) (2008) 577–599.
[29] O. Nguyen, E.A. Repetto, M. Ortiz, R.A. Radovitzky, A cohesive model of fatigue crack growth, Int. J. Fract. 110 (4) (2001) 351–369.
[30] M.Y. Wang, X. Wang, D. Guo, A level set method for structural topology optimization, Comput. Methods Appl. Mech. Eng. 192 (1–2) (2003) 227–246.
[31] G. Abaqus, Abaqus 6.11. Dassault Systemes Simulia Corporation, Providence, RI, USA, 2011.
[32] Q. Gao, H. Xin, J. A.F.O. Correia, A.S. Mosallam, F. Berto, Probabilistic fatigue life analysis considering mean stress effects of fiber reinforced polymer (FRP) composites, Int. J. Fatigue 162 (2022) 106951.
[33] A. Fernández-Canteli, C. Przybilla, M. Nogal, M.L. Aenlle, E. Castillo, ProFatigue: A software program for probabilistic assessment of experimental fatigue data sets, Procedia Engineering 74 (2014) 236–241.